Adsorption mechanism of 1,2-dichloroethane into an organophilic zeolite mordenite: A combined diffractometric and gas chromatographic study

Adsorption mechanism of 1,2-dichloroethane into an organophilic zeolite mordenite: A combined diffractometric and gas chromatographic study

Annalisa Martucci[a], Luisa Pasti[b], Marianna Nassi[b], Alberto Alberti[a], Rossella Arletti[c], Roberto Bagatin[d], Rodolfo Vignola[d], Rosalba Sticca[d]

[a]Earth Sciences Department, University of Ferrara, Via G. Saragat 1, 44100 Ferrara, Italy

[b]Department of Chemistry, University of Ferrara, Via L. Borsari 46, 44100 Ferrara, Italy

[c]Dipartimento di Scienze Mineralogiche e Petrologiche, University of Torino, Via Valperga Caluso 35, I-10125 Torino, Italy

[d]Research Centre for Non-Conventional Energy – Istituto Eni Donegani Environmental Technologies, Via Fauser 4, I-28100 Novara, Italy

Abstract

We investigated the 1,2-dichloroethane (DCE) adsorption process into an organophilic zeolite mordenite. A combined diffractometric, thermogravimetric and gas chromatographic approach enabled to obtain clear evidence of DCE adsorption in mordenite channels as well as to pinpoint the exact location of the organic species found in the structure. Rietveld refinement revealed the incorporation of 2.5 DCE molecules and approximately 4 water molecules within the mordenite channel system, in very good agreement with the weight loss given by TG analysis and the saturation capacity determined by the adsorption isotherm. This relevant incorporation of DCE molecules caused a remarkable increase in the dimension of the 12-ring, when compared to the parent zeolite. The distances between the oxygen atoms of the water molecules from the chlorine atoms of the organic molecule (W–Cl1 = 2.34 Å, W–Cl2 = 2.53 Å) suggest that different DCE molecules could be connected by means of hydrogen bonds through water, to form a DCE and water molecule complex. The isotherm adsorption model for organic compounds from an aqueous dilute solution was selected based on the results of the structural investigation.

Graphical abstract

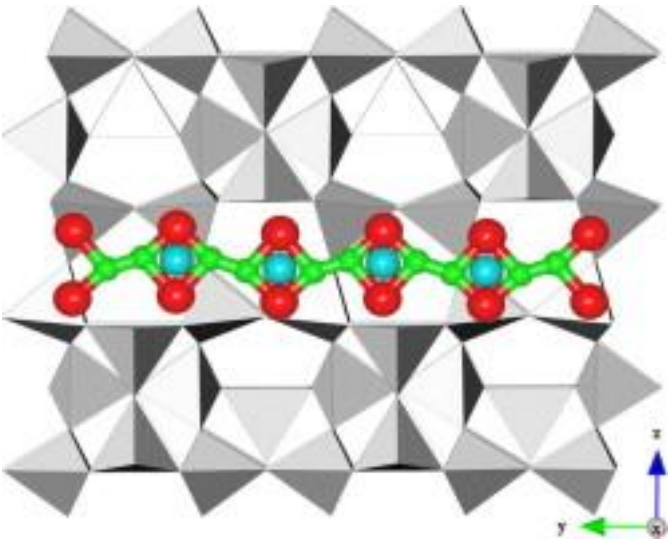

Highlights

Evidences of DCE adsorption into mordenite are reported.
2.5 DCE and 4 water molecules were adsorbed into the mordenite framework.
The adsorption of DCE into mordenite caused distortions of the 12-ring channels.

Keywords

- Mordenite;
- 1,2-Dichloroethane;
- Adsorption;
- Gas chromatography;
- X-ray diffraction

1. Introduction

Chlorinated volatile organic compounds (VOCs), such as dichloromethane (DCM) and 1,2-dichloroethane (DCE) constitute an important environmental pollutants class due to their high toxicity, inertness and widespread application in industry. Such compounds are typically carcinogens, mutagens and teratogens, and, furthermore, are involved in the destruction of the ozone layer. Substantial quantities of DCE are generated in vinyl chloride production plants [1] and are present in air stripping and soil venting remediation off-gases [2]. Other sources of entry into the ecosystem include effluent discharge from industries that use or produce DCE, effluents from the treatment of contaminated groundwater, air emissions and leachates from waste disposal sites, and long-range atmospheric transportation from remote sources. Despite DCE being the most abundant chlorinated groundwater pollutant on Earth, an efficient reductive in situ detoxification technology for this compound is not known. For instance, zero-valent iron (ZVI), which directly degrades several contaminants appears to be ineffective on irreducible compounds such as DCE, chlorobenzenes, as well as hydrocarbons [3] and [4]. Granular activated carbon (GAC) has been shown to be only slightly effective in treating water containing very soluble compounds, such as oxygenated organics, or low molecular weight compounds, such as DCE and vinyl chloride (VC) [5]. Recently Vignola et al. [6] have demonstrated that hydrophobic zeolites are able to effectively adsorb molecules against which ZVI or GAC are totally ineffective. In particular, ZSM-5 zeolite turned out to be suitable for mono-aromatic molecules, such as BTEX (benzene, toluene, ethylbenzene and xylene) and halogen–benzene derivatives [6].

The DCE molecule has been the subject of a considerable number of studies because of interest in its restricted internal rotation and the nature of the potential barrier associated with this motion. DCE is a small, flexible molecule which occurs in two stable conformations, namely *gauche* (with a Cl–C–C–Cl dihedral angle of ±60°) and *trans* or *anti* (with a Cl–C–C–Cl dihedral angle of 180°), respectively. Experimental and theoretical molecular conformational studies in ambient conditions have revealed that in the gaseous phase, DCE exists mainly in the *trans* conformer, due to the steric effect, which is basically composed of exchange and Coulombic repulsion [7], [8], [9], [10], [11] and [12]. In the liquid phase or in a polar solvent media, such as water, the dipole–dipole interactions with neighbouring species (in liquid) or polar solvent molecules (in solutions) stabilise the *gauche* conformer (with a dipole moment of 3.5 Debye) when compared to the *trans* conformer (with a near to zero dipole moment) [13], [14], [15], [16] and [17].

It is well known that the conformational equilibrium of molecules or atomic clusters can show strong differences in confinement, due to reduced dimensionality and large interface effects. In particular, the present work deals with the confinement effect of zeolite materials. Due to their confinement effect, zeolites and inorganic mesoporous materials can be described as solid solvents, as the electronegative charge on their framework can polarise adsorbed molecules as with any polar solvent [18]. The wide applicability of zeolites stems from their structural and compositional properties, such as their pore structures, acidic properties, good thermal stability and ion exchange properties [19], [20], [21], [22] and [23]. The ability of zeolites with a low Si/Al ratio to remove cations by ionic exchange has been largely demonstrated and utilised in water treatment plants producing drinking water [24]. In contrast, zeolites characterised by a high Si/Al ratio are hydrophobic and organophilic materials which are widely used in adsorption-related applications [25],

[26] and [27]. In fact, zeolitic networks of well-defined micropores may act as adsorption and reaction sites whose selectivity and activity can be modulated by acting on their structure and chemical composition. In selecting adsorbent materials, it is important to characterise their sorbent properties and this is usually done by modelling the experimental data with an adsorption isotherm model. However, to date several isotherms have been employed to interpret this phenomenon and in many cases the choice of model is based solely on the goodness of fit. In the present work, a structural investigation was performed to highlight the adsorption mechanisms in order to select the appropriate isotherm model.

X-ray and neutron diffraction techniques are usually employed to characterise the structure of zeolites loaded with hydrocarbon guest species in order to clearly locate their position inside the channel system [28], [29], [30], [31], [32], [33], [34], [35] and [36]. Unfortunately, these experiments are generally performed at low temperatures by incorporating hydrocarbons using the gas phase. However, pore diffusion through the gas phase is much faster than the liquid phase, especially in the case of highly volatile hydrocarbons which have rather large distribution coefficients. To date, studies and applications on organic pollutant adsorption in microporous zeolitic materials from aqueous media have been relatively scarce [26], [27], [37] and [38]. The presence of a small amount of water reduces the adsorption capacity of alkanes and olefins in zeolites, especially at low adsorbate concentration [39]. In particular, water decreases saturated hydrocarbons diffusivity, thus acting as a screen between the cationic sites of the zeolite and the hydrocarbon molecules (screening effect) and reducing both the sorption volume (steric effect) and the zeolite window apertures of the (blocking effect) [40], [41] and [42]. Beauvais et al. [42] reported a Monte Carlo molecular simulation study of the equilibrium adsorption of water and aromatics in zeolite faujasite NaY and observed cation redistribution upon water adsorption. The authors observed the same phenomenon in the presence of adsorbed xylene molecules in the noted. These results clearly show that the location of hydrocarbons and of chlorinated organics in zeolites has not been explored in detail, especially in the presence of water.

H-mordenite and chemically dealuminated H–Y zeolites resulted as the most active catalysts for chlorinated VOC destruction due to the presence of strong Brønsted acidity [22] and [23]. Mordenite (MOR) is a natural or synthetic zeolite, with an idealised chemical composition $Na_8Al_8Si_{40}O_{96}{\cdot}24H_2O$Na8Al8Si40O96·24H2O whose framework can be built up by the assembly of single 6-ring sheets linked by single 4-rings, or else by a combination of 5–1 secondary building units (SBUs). Its structure is characterised by straight 12-membered and 8-membered rings running along the *c* axis, and sinusoidal 8-membered rings running along the *b* axis; these channels accommodate extra framework cations and water molecules. The 12-ring channels are interconnected along [0 1 0] through 8-ring side pockets. In naturally occurring mordenites, the Si/Al ratio is within the range 4.3–6.0, whereas in synthetic mordenites this ratio varies from less than 5.0 up to 200 [54]. From a technical point of view, two different varieties of mordenite can be distinguished: Large Port (LPM) and Small Port Mordenites (SPM). Large Port Mordenites are hydrothermally synthesised in the Na-form between 75 and 260 °C, whereas Small Port Mordenites are usually hydrothermally synthesised between 275 and 300 °C [43]. Molecules with a diameter >4.5 Å can be introduced into large LPM channels, whereas SPM only accepts molecules with a diameter <4.2 Å and is thus less favourable for industrial applications [44]. As far as concerns its morphology, natural mordenite is characterised by acicular crystals with *c*-elongation, which are usually thin in the [0 1 0] direction, whereas synthetic mordenite commonly crystallises as large platelets with dominant (0 0 1) faces [45]. It seems that morphology is an additional parameter influencing small-port and large-port behaviour; in fact, platy mordenite enables easy access to large 12-membered ring channels, whereas long prismatic or fibrous (along *c*) crystals have fewer large-channel openings and diffusion is more sluggish [46] and [47]. In addition, most natural mordenites have properties which are characteristic of small-port mordenite.

The aluminosilicate framework of mordenite has orthorhombic topology with C*mcm* symmetry and includes four symmetrically independent tetrahedral cation sites and 10 framework oxygen sites. In the natural mineral real symmetry is reduced to C$mc2_1$ [48] and [49] in order not to constrain the O8 oxygen on the inversion centre, and consequently, to avoid a straight T–O–T angle. However, the crystal structure remains strongly C*mcm* pseudo-centrosymmetric so that all structure refinements of natural, synthetic and H-mordenite were performed in this space group [50], [51] and [52]. Dehydrated, cation-exchanged mordenite occurs with a P*bcn* space group [52] and [53] whereas hydrated, cation- and molecule-exchanged samples have been refined in lower monoclinic symmetry with the C*c* space group [49] and [54].

Recently, it has been proved that host–guest interactions in zeolitic systems have a strong influence on the conformational properties of adsorbed organic molecules due to the effect of the zeolite framework [55]. Therefore, it is important to understand the guest molecules behaviour inside the zeolite hosts in applications involving guest species adsorption in zeolitic frameworks, since it can influence the thermodynamics and kinetics of the adsorption processes.

For the first time this study reports the adsorption of both 1,2-dichloroethane and water into an organophilic zeolite mordenite from dilute solutions. To date, no information is available on the mechanisms and effectiveness of high-silica mordenite for DCE removal from water and no studies have investigated the effects of adsorbed DCE on the zeolite pore size. These results enabled an isotherm model which better explains the experimental adsorption data to be selected. A combined diffractometric, thermogravimetric and gas chromatographic study was used to:

1) Investigate the adsorptive properties of hydrophobic synthetic mordenite.
2) Characterise its structure after DCE adsorption.
3) Localise the organic species in the mordenite channel system.
4) Investigate DCE conformational equilibrium in this organophilic zeolite.
5) Probe the interactions between DCE molecules, water molecules and framework oxygen atoms.

2. Experimental

2.1. Materials

1,2-Dichloroethane (purity 99.8%) and sodium chloride (purity 98%) were obtained from Sigma–Aldrich (Steinheim, Germany). The as-synthesised mordenite sample is a hydrophobic commercial adsorbent, which is synthesised with SiO_2/Al_2O_3 as equal to 200, and was purchased in its protonated form (HSZ-690HOA Tosoh Corporation). Its Na_2O content was lower than 0.1 wt.%. The material characteristics are reported in Fig. 1. The water used was filtered and purified by reverse osmosis using Milli-Q apparatus (Millipore, MA, USA).

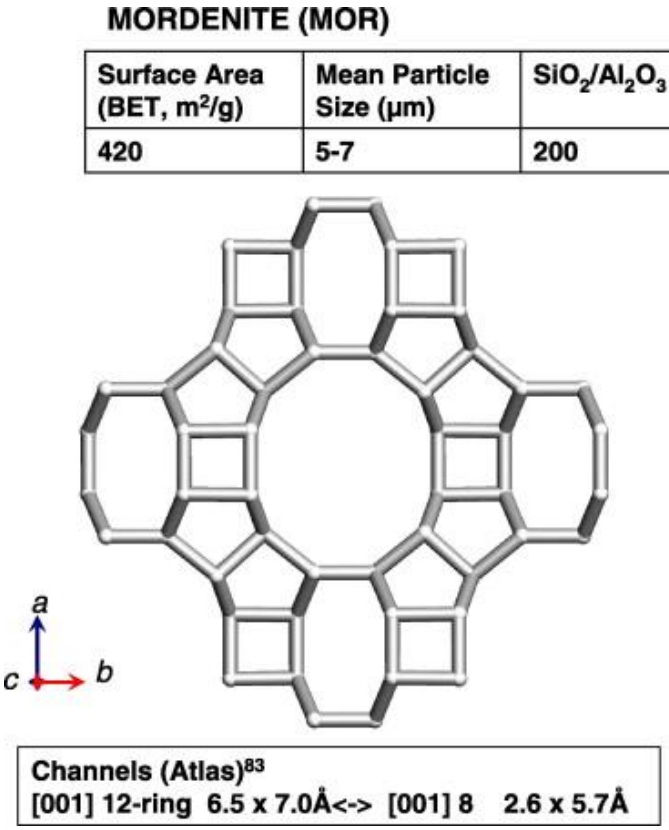

Fig. 1. Structure and characteristics of zeolite mordenite under investigation.

The solid-phase microextraction (SPME) fibres which were used were coated with polydimethylsiloxane (PDMS) at 100 μm thickness (supplied by Supelco, PA, USA) and housed in a manual holder (Supelco, PA, USA). The fibre sorbent was selected due to its high versatility; in fact, it is generally used for the extraction of a wider range of analytes with differing polarity and volatility. Following the guidelines, the fibres were conditioned under helium at a flow-rate of approximately 1.0 mL/min with the split valve open (to reduce the amount of impurities entering the column) in the hot injection port of a gas chromatograph at 250 °C for 1 h prior to use. Additionally, the SPME fibres were conditioned for 15 min at 250 °C every day before use and were systematically cleaned at 250 °C for 20–30 min after every extraction. The blanks were tested by thermal desorption (5 min in the injection port) followed by gas chromatography (GC).

2.2. Scanning electron microscopy (SEM)

SEM images of the zeolites were acquired using a Zeiss EVO 40 XVP scanning electron microscope. To prepare the sample for SEM, a drop of dilute colloidal solution of the sample was dripped onto the SEM sample stud surface and the sample stud was then dried at 60 °C for 3 h. Shortly before SEM image acquisition, the latter was coated with gold. The SEM zeolite image reported in Fig. 2 indicated that mordenite is composed of particles with lamellar or plated morphology, the lamella lengths are in the 2–3 μm range.

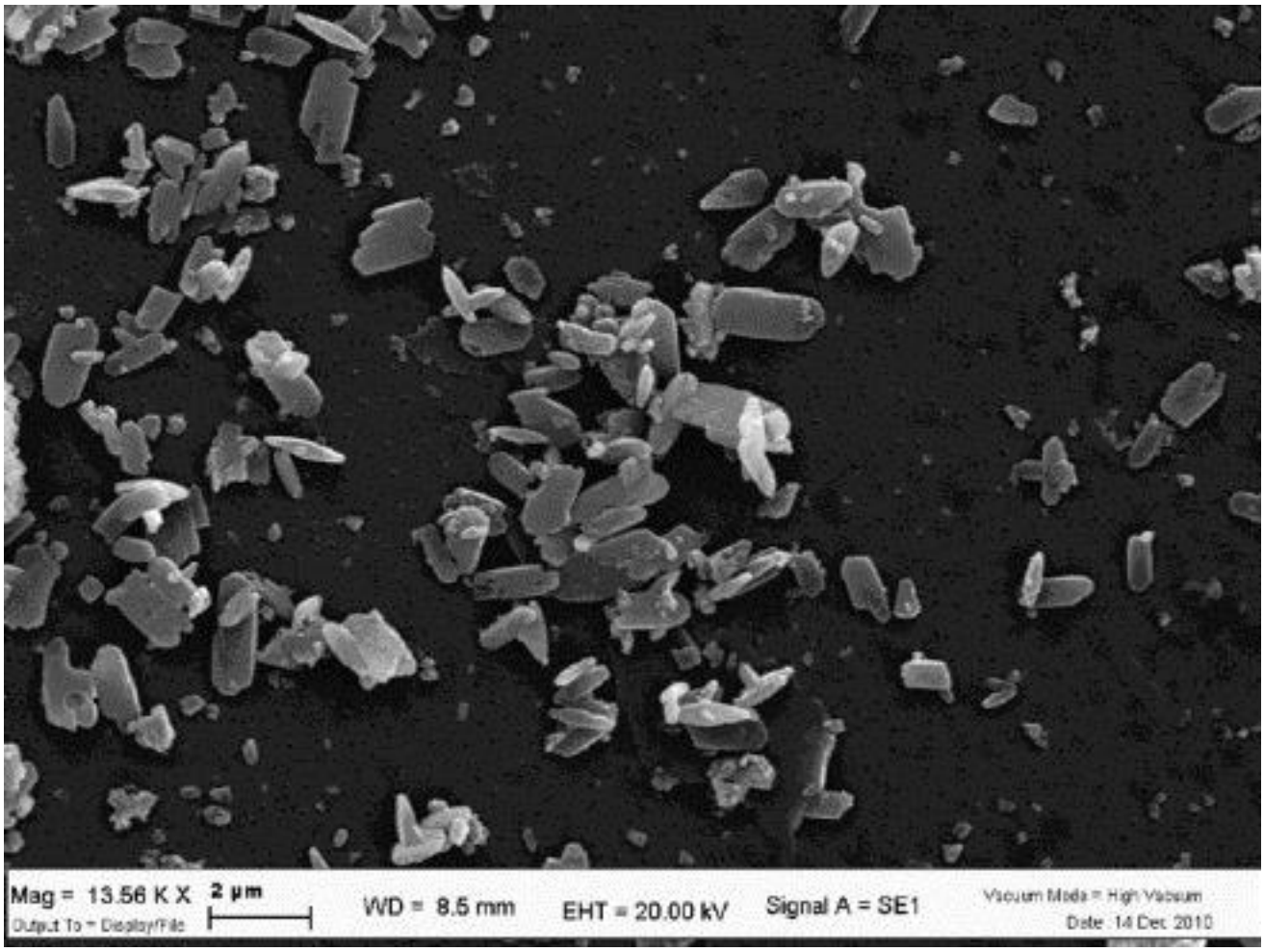

Fig. 2. Scanning electron microscopy (SEM) image of zeolite mordenite showing large platelets with dominant (0 0 1) faces.

2.3. X-ray diffraction

A mordenite powder pattern after DCE adsorption (MOR-DCE) was measured on a Bruker D8 Advance Diffractometer equipped with a Sol-X detector, using Cu $K_{\alpha1,\alpha2}$ radiation in the 4–116° 2θ range and a counting time of 12 s/step.

2.4. Structure determination and refinement strategy

The diffraction pattern was firstly indexed using the DICVOL program [56] in an orthorhombic cell [a = 18.041 Å, b = 20.212 Å, c = 7.447 Å, V = 2715.5 Å^3]. Rietveld structure refinement was therefore performed, using the GSAS package [57] with the EXPGUI interface [58]. The framework atoms for hydrophobic mordenite reported by Martucci et al. [27] provided the initial parameters for structure determination. All tetrahedral sites were modelled with Si atoms, while the amount of Al atoms were neglected. In all the Rietveld structure refinement, the Bragg peak profile was modelled using a pseudo-Voigt peak-shape function [59] with 0.01% cut-off peak intensity. The background curve was fitted using a Chebyschev polynomial with 20 variable coefficients. The 2θ-zero shift was accurately refined into the data set pattern. The scale factor and unit-cell parameters were allowed to vary in all the cycles. The refined structural parameters for the data histogram were the following: fractional coordinates and isotropic displacement factors for all atoms (one for each tetrahedral site and framework oxygen atom), and occupancy factors for the extraframework ions. Occupancy factors and isotropic displacement factors were varied in alternate cycles. Soft constraints were imposed on the tetrahedral cations and coordinated framework oxygen atom T–O distances during the first stages of refinement, and left free in the last cycles. The positions of the extraframework sites were determined by the Fourier and Difference Fourier maps. The crystallographic data and refinement details are reported in Table 1. The final atomic positions, thermal parameters and occupancies are given in Table 2, the interatomic distances and angles in Table 3. The final observed and calculated patterns are shown in Fig. 3.

Table 1. Lattice parameters and refinement details for mordenite before (MOR) and after DCE adsorption (MOR-DCE).

	MOR	**MOR-DCE**
Space group	Orthorhombic, C*mcm*	Orthorhombic, C*mcm*
a (Å)	18.069(1)	18.075(1)
b (Å)	20.219(1)	20.234(1)
c (Å)	7.456(3)	7.4602(2)
$\alpha = \beta = \gamma$ (°)	90	90
V (Å^3)	2723.9(2)	2728.3(2)
Wavelength of incident radiation (Å)	1.5417(1)	1.5417(1)
Refined pattern 2θ range (°)	4–116	4–116
Profile function	T–C–H pseudo-Voigt correction	T–C–H pseudo-Voigt correction
H-atom treatment	Not refined	Not refined
R_{wp} (%)	9.82	12.6
R_p (%)	7.45	9.8
R_F^2 RF2 (%)	6.42	8.4
No. of contributing reflections	2246	2302
N_{obs}	5665	5584
N_{var}	47	65

Estimated standard deviations in parentheses refer to the last digit.

Table 2. MOR-DCE atomic coordinates, occupancies and thermal parameters.

Atom	***x*/*a***	***y*/*b***	***z*/*c***	**Multiplicity**	**Fraction**	**Uiso**
T1	0.3068(3)	0.0752(2)	0.0401(5)	16	1.0	0.010(1)
T2	0.3051(3)	0.3103(2)	0.0447(6)	16	1.0	0.010(1)
T3	0.0852(4)	0.3786(4)	0.25	8	1.0	0.010(1)
T4	0.0843(4)	0.2205(4)	0.25	8	1.0	0.010(1)
O1	0.1190(4)	0.4076(5)	0.4326(9)	16	1.0	0.014(2)
O2	0.1229(4)	0.1874(5)	0.4212(11)	16	1.0	0.014(2)
O3	0.2368(4)	0.1215(4)	0.9973(13)	16	1.0	0.014(2)
O4	0.0910(7)	0.2959(3)	0.25	8	1.0	0.014(2)
O5	0.1676(7)	0.1898(10)	0.75	8	1.0	0.014(2)
O6	0.1727(8)	0.4216(8)	0.75	8	1.0	0.014(2)
O7	0.2158(8)	0.5	0.5	8	1.0	0.014(2)
O8	0.25	0.25	0.5	8	1.0	0.014(2)
O9	0	0.4011(10)	0.25	4	1.0	0.014(2)
O10	0	0.1957(11)	0.25	4	1.0	0.014(2)
Cl1	0.5	0.4287(17)	0.25	4	0.30(1)	0.16(1)
Cl2	0.5	0.5566(26)	0.25	4	0.31(1)	0.15(1)
C	0.5	0.4927(21)	0.0918(13)	8	0.33(1)	0.14(1)
W	0.3861(15)	0.4840(17)	0.25	8	0.48(1)	0.09(1)

Table 3. Selected bond distances (Å) and angles (°) for mordenite before (MOR) and after DCE adsorption (MOR-DCE).

	MOR	**MOR-DCE**		**MOR**	**MOR-DCE**
T1–O1	1.599(2)	1.602(2)	T2–O2	1.600(2)	1.597(2)
T1–O3	1.605(2)	1.607(2)	T2–O3	1.606(2)	1.606(3)
T1–O6	1.613(1)	1.610(2)	T2–O5	1.601(2)	1.610(2)
T1–O7	1.599(2)	1.602(2)	T2–O8	1.605(2)	1.608(3)
T3–O1 [x2]	1.602(2)	1.603(2)	T4–O2[x2]	1.606(2)	1.602(2)
T3–O4	1.610(2)	1.604(2)	T4–O2	1.609(2)	1.605(2)
T3–O9	1.613(2)	1.605(2)	T4–O10	1.610(2)	1.604(3)
T1–O1–T3	151.3(8)	145.5(8)	T1–O6–T1	147.4(11)	153.0(12)
T2–O2–T4	143.4(8)	143.4(8)	T1–O7–T1	142.6(10)	150.5(11)
T1–O3–T2	152.5(7)	155.7(7)	T2–O8–T2	180	180
T3–O4–T4	172.5(9)	171.9(9)	T3–O9–T3	162.8(16)	147.2(17)
T2–O5–T2	150.1(8)	144.2(10)	T4–O10–T4	135.2(16)	143.6(18)
C–Cl1		1.75(1)	Cl1–Cl2		2.59(2)
C–Cl2		1.75(1)	Cl2–W		2.53(4)
C–C		1.40(1)	Cl1–W		2.34(4)
Cl2–O10		2.81(5)	C–W		2.38(3)

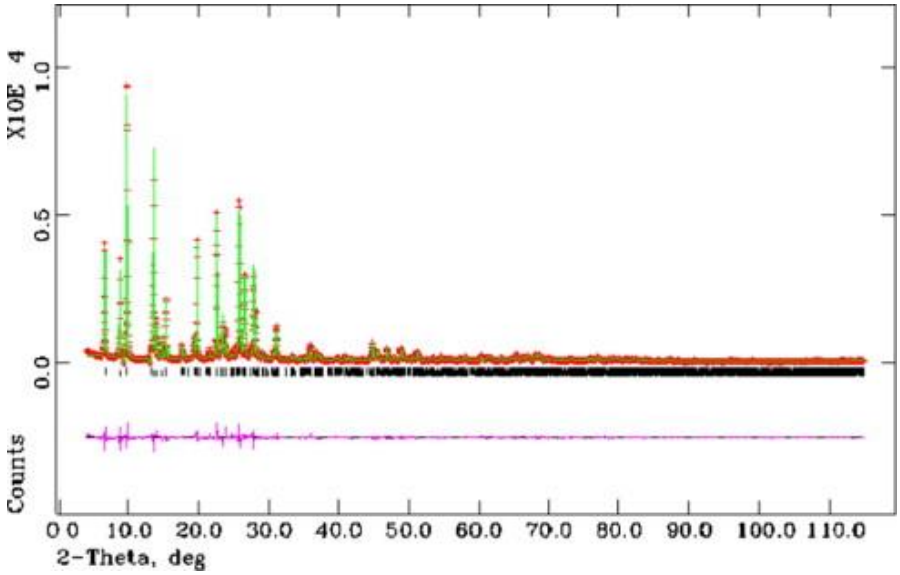

Fig. 3. The observed (red), calculated (green), and difference (pink) profiles of MOR-DCE. (For interpretation of the references to colour in this figure legend, the reader is referred to the web version of this article.)

2.5. Thermal analyses

Thermogravimetric (TG), differential thermogravimetric (DTG) and differential thermal analyses (DTA) measurements of exhausted sample were performed in air at up to 1000 °C using an STA 409 PC LUXX® – Netzch at a 10 °C/min heating rate. The thermal curves are reported in Fig. 4.

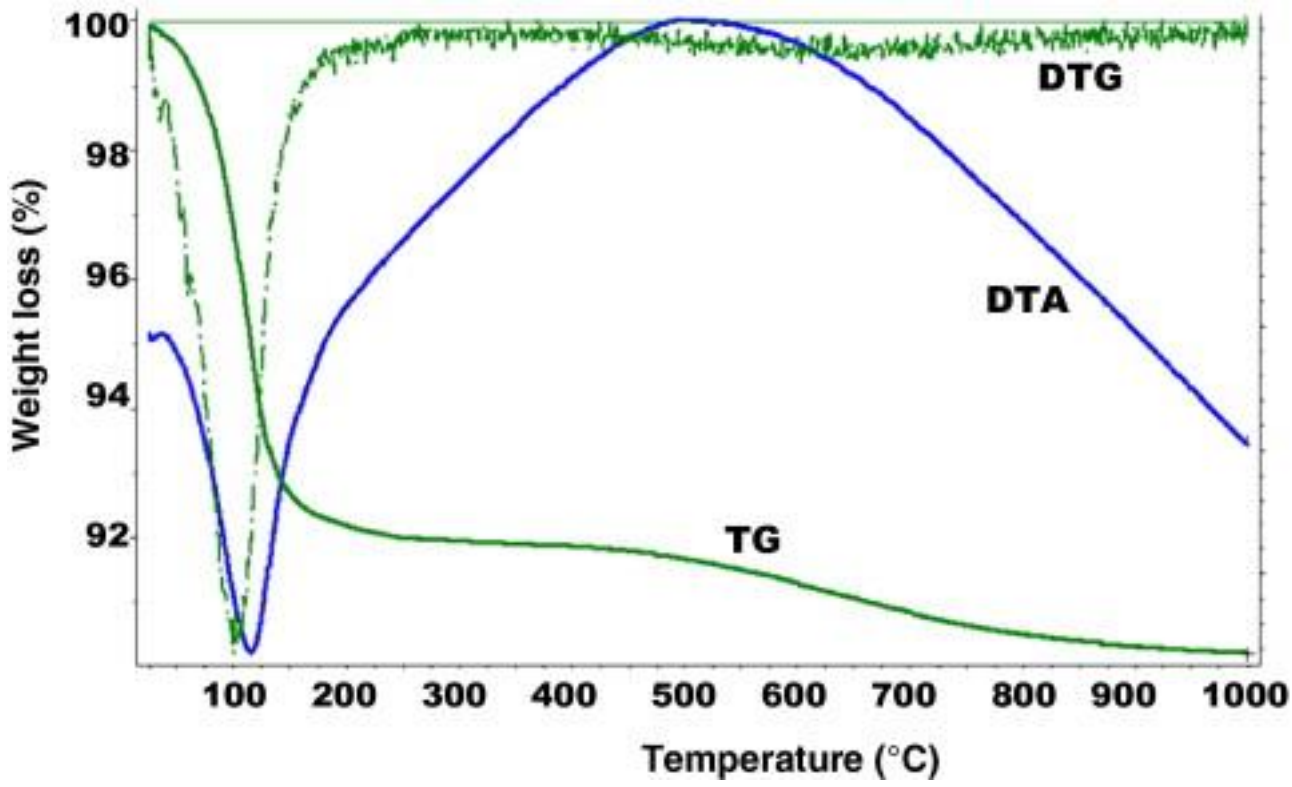

Fig. 4. Thermogravimetric (TG), differential thermogravimetric (DTG) and differential thermal (DTA) curves in mordenite after DCE-dry air atmosphere adsorption.

2.6. Gas chromatography

Headspace-gas chromatography (HS-SPME-GC) solid phase-micro extraction was used to extract 1–2-dichloroethane from each aqueous sample and to subsequently perform to GC analysis. Preliminary experiments were done in order to evaluate extraction conditions. The headspace (HS) mode was used for extraction from a sample volume of 10 mL of DCE solutions. The addition of an inorganic salt has often been used in order to enhance the activity coefficients of volatile components in aqueous solutions, increasing the concentration in the headspace vapour. In the present work, 2 mL of a sodium chloride solution (300 g/L) were added to the sample which was placed in 25 mL glass flasks sealed with Teflon screw caps. After equilibration at 40(±0.5) °C, for 10 min, the SPME was inserted and the samples were maintained under controlled agitation with a magnetic stirrer (300 rpm) for 10 min. Finally, the fibre was inserted into the GC injector for analysis. The desorption time was 1 min.

The GC used in this work was an HRGC 5160 MEGA SERIES Instrument (Carlo Erba, Mi, I) equipped with a split/splitless injector and an electron capture detector (ECD, ^{63}Ni). A fused-silica DB-5 capillary column (60 m × 0.25 mm ID: 0.25 μm film thickness; J&W Scientific, USA) was employed. Helium (99.999%) was used as a carrier gas at a constant head pressure of 50 kPa and nitrogen (196 kPa) was employed as a make-up gas at a constant flow-rate (1 mL/min). The detector and injector temperatures were held constant at 250 °C. The GC oven was programmed as follows: 40 °C (5 min), 5 °C/min–80 °C (5 min), 30 °C/min–100 °C (5 min). The linearity of the quantitative analysis method was tested by evaluating the calibration curves: standard solutions of DCE in MilliQ water were analysed at varying concentration levels in the range 0.1–30 ppm. Each concentration was analysed twice. The linearity range as well as the method detection limit (LOD) were evaluated and computed from the calibration line. Good linearity was observed with a correlation coefficient of 0.993.

2.7. Adsorption isotherm

The adsorption equilibrium isotherm was determined using the batch method. Batch experiments were carried out in duplicate in 25 mL crimp top reaction glass flasks sealed with PTFE septa (Supelco, PA, USA). The flasks were filled in order to have minimum headspace, a solid/solution ratio (mg mL^{-1}) of 1:4 was employed. After equilibration (24 h) at a temperature of 25.3 ± 0.5 °C under stirring, the solids were separated from the aqueous solution by centrifugation (10,000 rpm for 30 min) and analysed by HS-SPME-GC, as above described.

3. Results and discussion

As described in the experimental section, the MOR particles are characterised by lamellar or plated morphology. This morphology enables easy access to the large 12-membered ring channels, thus indicating that the sample has properties which are characteristic of Large Port Mordenite.

The experimental data of the adsorption isotherm are reported in Fig. 5. In this work, the experimental sorption data were modelled using the traditional Langmuir isotherm [60]:

$$q = \frac{q_s K_L C_e}{1 + K_L C_e}$$

where q (mg g^{-1}) is the equilibrium adsorbed concentration, C_e (mg L^{-1}) is the equilibrium concentration in water, K_L (L mg^{-1}) is the Langmuir coefficient (binding constant), and q_s (mg g^{-1}) the saturation capacity. K_L and q_s, were determined by non-linear least squares data fitting. It can be seen that the examined concentration range is well fitted using the Langmuir equation (see Fig. 5a). The parameters obtained by fitting the Freundlich equation $q = KC_e^{1/n}$ q=KCe1/n are also reported in Table 4. In several papers devoted to adsorption from dilute solutions, Dubinin–Astakhov (DA) or Dubinin–Radushkevich (DR)

adsorption isotherms have been applied. The Dubinin–Astakhov equation was derived from Polanyi's potential theory for a vapour phase system and extended from Manes [61] to aqueous systems by defining the Polanyi adsorption potential $\varepsilon_{SW}=RT\ln(S/C_e)$εSW=RTln(S/Ce), where RR is the ideal gas constant (J mol^{-1} K^{-1}), *T* the temperature (K), and *S* is the water solubility (mg L^{-1}). The Polanyi–Dubinin–Manes (PDM) model [62] is given by:

$$q = V_0 \rho_0 \exp\left[\frac{RT \ln S/C_e}{E}\right]^b$$

where V_0V0 and ρ_0ρ0 are the maximum volume of adsorbed compound for unit mass of adsorbent (cm^3 g^{-1}) and compound density (mg cm^{-3}), respectively. EE (kJ mol^{-1}) is the free energy of the adsorption process compared to that of a reference compound [63]. bb is an exponent which can be obtained by fitting or set to a given (integer) value, when b=2b=2 it becomes the Dubinin–Radushkevich equation. To apply Eq. (2), the water solubility of 1,2-dichloroethane was set to 8700 mg L^{-1}, DCE had a vapour pressure of 81 hPa at 20 °C, a log K_{ow} of 1.45, and a density of 1.25 (g cm^{-3}) [64]. In Fig. 5b it can be seen that the experimental data are well fitted using the PDM model. From the data in Table 4, it is possible to infer some adsorption process properties. It can be noted that the saturation capacity evaluated from Eq. (1) is 71.5 mg g^{-1} and that this value is in agreement with the pore volume obtained from fitting the PDM model Eq. (2), but that it is smaller than the mordenite pore volume. The *b* value Eq. (2) obtained for the zeolite is about 4. This result is indicative of relatively homogeneous adsorbents with narrow site energy distribution, and is in agreement with the literature data on Y zeolite [65]. The exponent parameter of the Freundlich equation is in agreement with those found for VOC [66]. In Table 4, it is notable that the goodness of fit (coefficient of determination) for the three models employed are similar. Therefore, the choice of the model based solely on statistical parameters of fitting seems to be arbitrary. From the literature data, it seems that the micropore-filling-based PDM isotherm should theoretically be the best model to describe the sorption process on microporous materials. However, it has been found that the PDM isotherm underestimates pore volume at a low aqueous concentration range (<2 mg/L). This result was also found in TCE sorption on other adsorbents [67]. This was supposed to be due to another sorption mechanism in addition to micropore-filling at low concentrations, in particular due to specific sorbent sites of high adsorption energies. Moreover, loading results for trichloroethylene from both the liquid and vapour phase indicated that the liquid phase did not penetrate the silicalite-1 pores. However, it did enter the dealuminated NaY pores, even if theoretically, trichloroethylene can penetrate the pores of both the studied zeolites [67]. Finally, one unresolved issue from the aqueous solution adsorption experiments was if the presence of water affected the adsorption capacity, and whether or not the water actually entered the micropores. Therefore, there is no clear piece of evidence on which isotherm model to choose out of all these experimental results. This is mainly as a result of a lack of knowledge about adsorption mechanisms. In order to highlight the adsorption mechanism in use, a structural investigation was carried out.

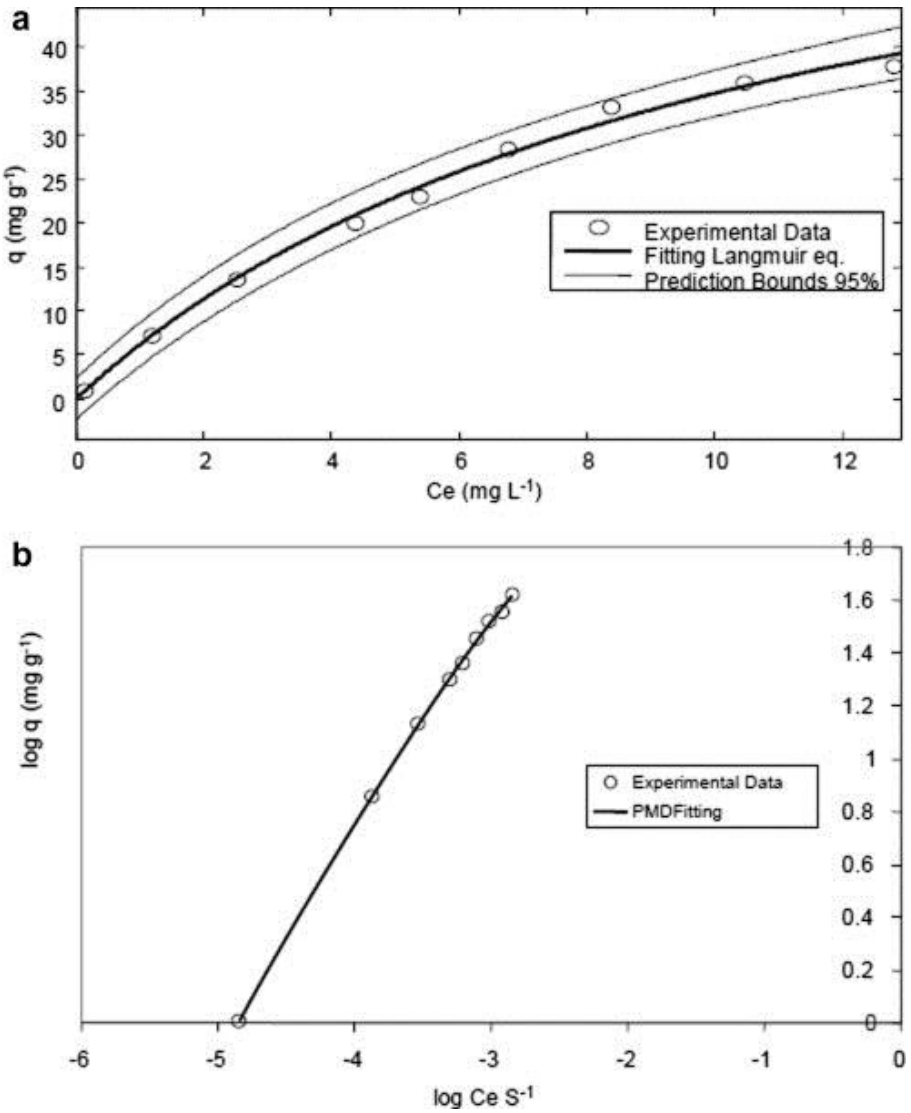

Fig. 5. Adsorption isotherm of DCE on MOR: Circle symbols: measured equilibrium concentrations; (a) solid line: fitted Langmuir equation; dashed lines: 95% confidence prediction bounds. (b) Solid line: fitted PMD equation.

Table 4. Fitting isotherms parameters obtained by fitting the experimental data in Fig. 5. The confidence limits at 95% of probability are reported in parentheses.

Langmuir			
K_L (L mg^{-1})	q_S (mg g^{-1})		R^2
0.09	71		
(0.065, 0.12)	(59, 84)		0.9942
Freundlich			
K (mg g^{-1})(L g^{-1})^n	n		R^2
7.9	1.6		
(6.0, 9.7)	(1.3, 1.8)		0.9832
PMD			
V_0 (cm^3 kg^{-1})	E (kJ mol^{-1})	b	R^2
62.5	18	4	0.9914
(49.4, 74.0)	(11, 26)		

Thermogravimetric analysis (TG) was used to determine the amount of DCE molecules embedded in the mordenite framework, and to monitor the decomposition process of organic molecules during the heating

procedure. The TG curve of the MOR-DCE shows a sudden change in its slope at about 90 °C, thus indicating the presence of molecules which are weakly bonded to the surface (water and/or DCE). The weight loss which occurred at higher temperatures (temperature range 200–700 °C), could indicate the decomposition and elimination of the organic molecules embedded in the mordenite channel system. Weight loss at 1000 °C is about 10% (see Fig. 4) in comparison to 7% of the as-synthesised material at the same temperature [27]. The question is, whether this variation is really due to DCE adsorption, which remarkably or completely substitutes H_2O in the as-synthesised material, or to a trapping of further water molecules from the aqueous solution.

A comparison of the X-ray diffraction patterns of as-synthesised (MOR) and mordenite after DCE adsorption (MOR-DCE) shows relevant differences both in the intensity and position of the diffraction peaks (Fig. 6), indicating that the mordenite crystal structure was markedly modified by the DCE adsorption experiment. Rietveld structure refinement indicated a small but significant increase of unit cell parameters in comparison to those of the untreated material (see Table 1) and revealed a relevant modification in the channel system (see Fig. 7). The 12-membered ring strongly increased and its Crystallographic Free Area (C.F.A.) *sensu* Baerlocher et al. [68] became 35.9 $Å^3$ as compared with the 33.0 $Å^3$ C.F.A. of the untreated mordenite. This increase was remarkably compensated by a decrease in the 8-membered ring (C.F.A. = 10.4 $Å^2$ in MOR-DCE, 11.8 $Å^2$ in MOR). These results clearly indicated that the increase in weight loss resulting from the DCE adsorption experiment was not only due to the trapping of other water molecules from the aqueous solution but also to a remarkable modification in the extraframework content, i.e. to the adsorption of a significant amount of DCE molecules.

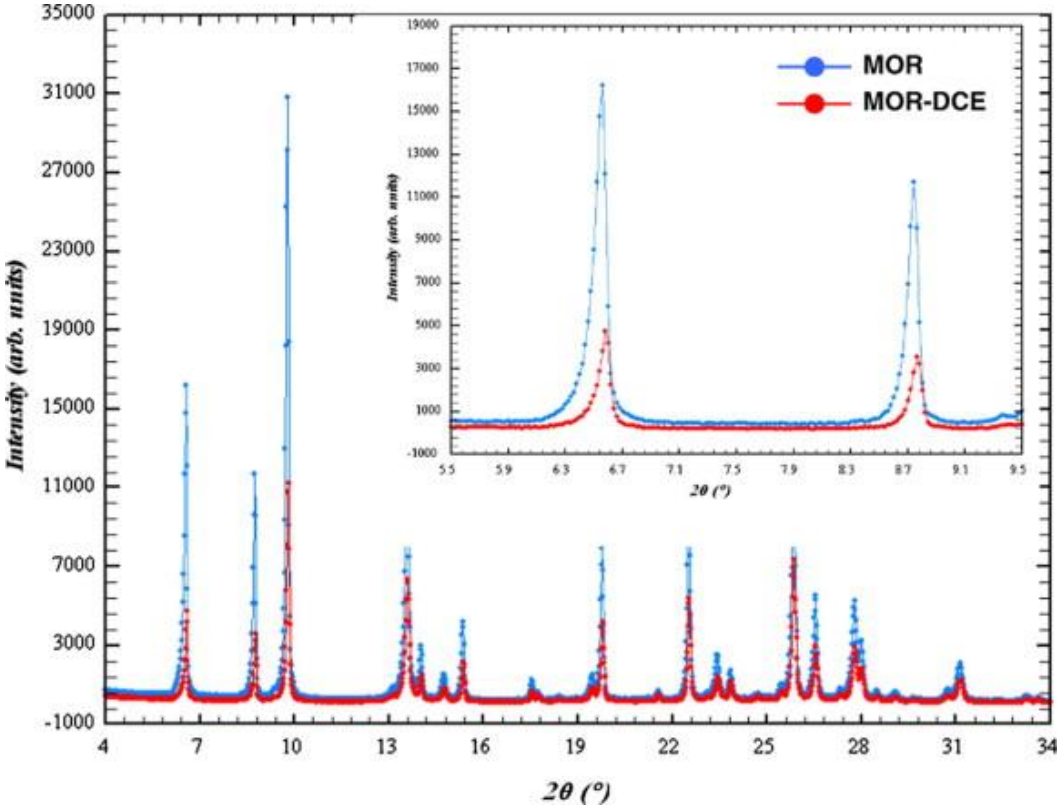

Fig. 6. Observed powder diffraction patterns of MOR (blue line), and MOR-DCE (red line), at low and intermediate 2θ angles, showing strong differences both in the intensity and position of the diffraction peaks. (For interpretation of the references to colour in this figure legend, the reader is referred to the web version of this article.)

12-RING	MOR	MOR-DCE
O10-O10	5.74(1)	6.10(1)
O2-O2	6.14(1)	6.17(1)
O3-O3	6.91(1)	7.17(1)
O7-O7	7.15(1)	7.59(1)
8-RING	**MOR**	**MOR-DCE**
O7-O7	5.41(1)	5.08(1)
O9-O9	3.01(1)	2.76(1)
O1-O1	3.20(1)	3.09(1)

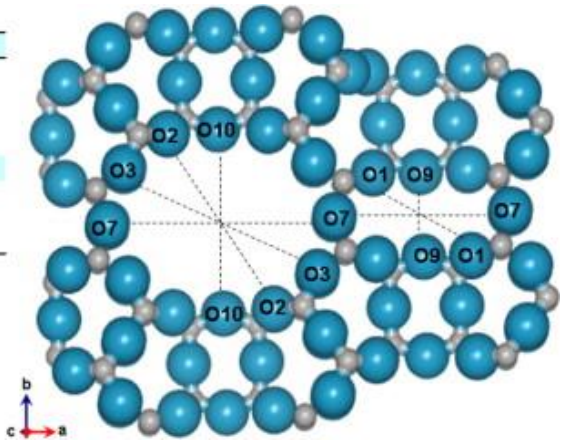

Fig. 7. Free diameter (Å) of the 12- and 8-ring channels of MOR and MOR-DCE, viewed normal to [0 0 1]. Oxygen is assumed to have an ionic radius of 1.35 Å.

The difference Fourier map generated using the GSAS package, revealed the presence of a number of extraframework ions inside the 12-ring channel. The two largest peaks in the difference Fourier map were attributed to chlorine atoms of encapsulated DCE molecules (Cl1 and Cl2 in Table 2 and Table 3). With this assumption, it was easy to localise a third peak to be attributed to a carbon atom (C in Table 2 and Table 3). Moreover, using this assumption, reasonable values were also obtained for C–C and C–Cl bond distances in the DCE molecule. The geometry of the DCE molecule, which was very near to ideal, as well as the very similar occupancy values (around 30%) and isotropic displacement parameters (Uiso ≈ 0.15 A^3) obtained for the carbon and chlorine atoms confirmed that the observed peaks had been correctly attributed to the DCE compound. Fig. 8 shows the location of these sites in the *Cmcm* space group. If Cl atoms only occupy Cl1 or Cl2 sites (referred to as "trans1" and "trans2", respectively in Fig. 8) DCE occurs in *trans*-configuration. Trans1 and trans2 configurations are not constrained by symmetry elements, so that only one of these could be present. However, the very similar occupancy levels for the Cl1 and Cl2 sites (Table 2) exclude this possibility. The dihedral angle between the Cl–C–C–Cl atoms, commonly referred to as ϕϕ, is 180°. On the contrary, when the Cl1 and Cl2 sites are contemporarily occupied, DCE occurs in *gauche*-configurations. The presence of symmetry elements of the *Cmcm* space group (inversion centre at ½, ½, ½ and diad at *x*, ½, ½) imposes the presence of two *gauche*-configurations, which are obviously not occupied at the same time, and are referred to as gauche1 and gauche2, respectively in Fig. 8. The dihedral angle between the Cl1–C–C–Cl2 atoms, is 60°. In conclusion, Rietveld structure refinements of exhausted mordenite, did not demonstrate whether only *trans*- or *gauche*-configurations were present or if both were present in different frequencies. Consequently, X-ray diffraction does not give a clear indication on the most favoured DCE configuration in mordenite structural confinement, but this is beyond the scope of this work. As reported previously, the occupancy of Cl and C atoms is only 30%, and consequently, DCE molecules, whatever their configuration, alternate randomly with non-occupied positions. Fig. 8 shows that DCE molecules run parallel to the *c* direction, i.e. along the 12-ring channel.

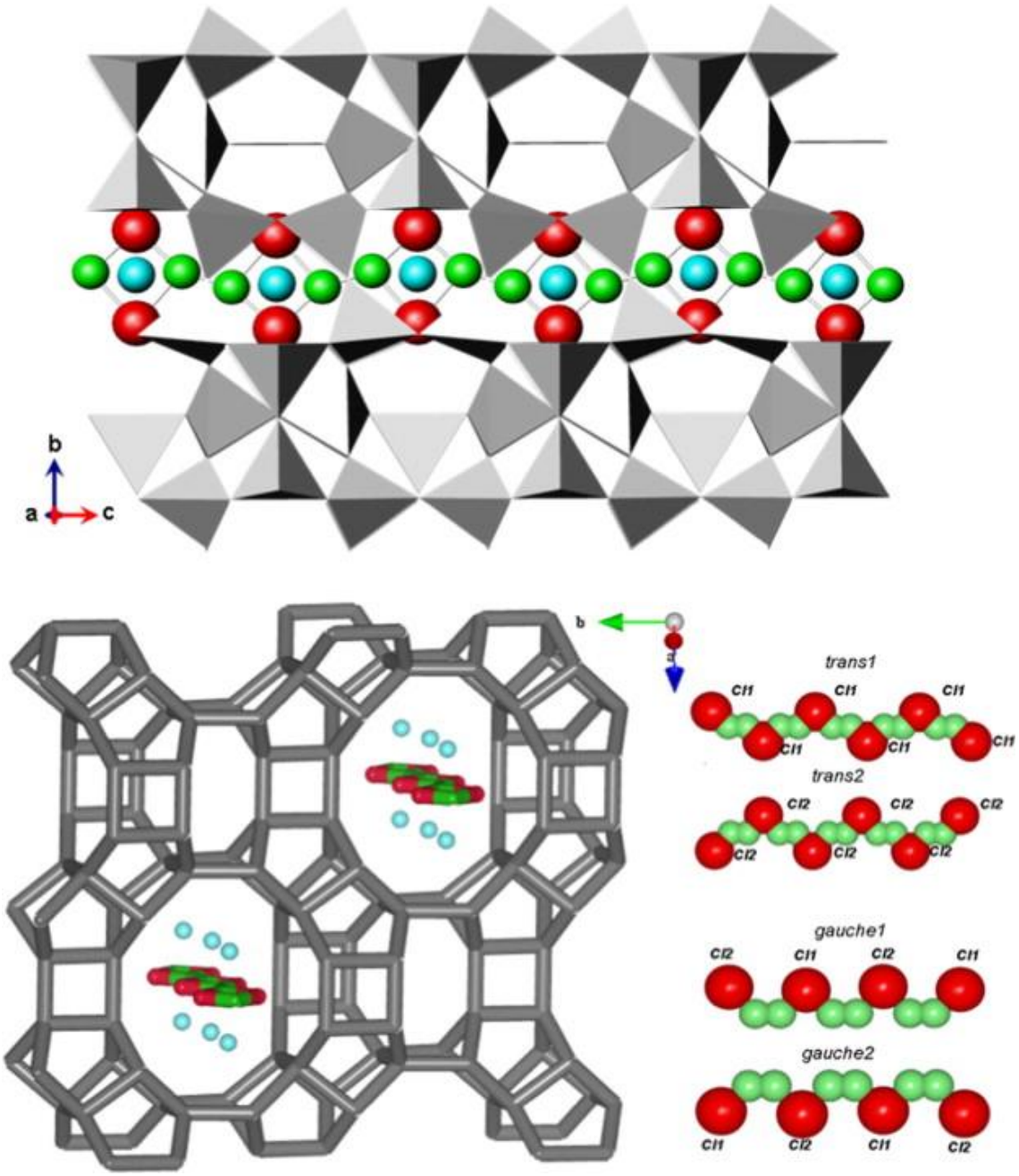

Fig. 8. MOR-DCE projections along [1 0 0] (top) and [0 0 1] (bottom) showing DCE (Cl represented with red, C with green spheres) and water molecules (with blue spheres) which run parallel to the *c* direction, i.e. along the 12-ring channel. (For interpretation of the references to colour in this figure legend, the reader is referred to the web version of this article.)

In MOR-DCE, the DCE molecule distance from the framework oxygens is larger than 3.5 Å, thus indicating the absence of electrostatic interaction with the framework. Only a few examples of molecule-framework contacts in zeolite or layered materials have been reported [[69] and references therein]. Most of them concern systems where the guest molecules are usually the templates used during the synthesis (often amine). When the guest molecules are introduced after synthesis, they are frequently disordered and, when localised, establish interactions with framework oxygen atoms which can be classified as medium to weak [[27] and references therein]. In particular, Porcher et al. [69] determined the crystal structure of mordenite after the inclusion of *p*-*N*,*N*-dimethylnitroaniline using synchrotron powder diffraction and showed that the guest molecules are located in the large 12-membered ring channel at the intersection with the 8-membered channel and form hydrogen bonds with the framework oxygens which delimitate the channels. The 12-membered-ring channels also host both thionin blue [49] and methylene blue molecules [54] which interact with the framework and show a strongly disordered arrangement.

The difference-Fourier map revealed the presence of a further extraframework site which was attributed to water molecules (W site). This site has a slightly higher level of occupancy than that of the organic molecules (Table 2). The importance of this W site is immediately clear: the distance of the oxygen atom in the water molecule from the organic molecule chlorine atoms (W–Cl1 = 2.34 Å, W–Cl2 = 2.53 Å, see Table 3) suggests that different DCE molecules could be connected by means of hydrogen bonds through W to form a complex of DCE and water molecules independently by *gauche* or *trans* DCE sequencing.

On the whole, 2.5 DCE molecules (which correspond about to 7.7% in weight) and approximately 4 water molecules (which correspond to approximately 2.3% in weight) were localised inside the mordenite channel system. Therefore, the structure refinement gave an extraframework content of about 10% in weight, which was in very good agreement with the weight loss given by TG analysis and with the saturation capacity determined by the adsorption isotherm.

To summarise, Rietveld refinement revealed a relevant level of incorporation of DCE molecule incorporation in the mordenite structure which caused a remarkable increase in the dimensions of the 12-membered ring where the DCE molecules were hosted (see Fig. 7 for details) when compared with those found in the parent zeolite. This clearly indicates that both *gauche*- and *trans*-conformers can be present. Wang and Huang [70] found that the *anti* or *trans* rotational conformer of 1-Bromo-2-chloroethane in organophilic silicalite-1 and siliceous Y zeolites prevails at room temperature, whereas the *gauche* conformer is the dominant conformer in hydrophilic L and Na-Y zeolites. Since 1-bromo-2-chloroethane differs from DCE only by one Br atom and consequently, has a lower dipole moment and higher steric hindrance, it seems reasonable to assume a *trans* (*anti*) conformation for DCE in MOR. Moreover, a *trans* DCE conformer is favoured in other organophobic zeolites such as ferrierite and L zeolites [71].

From the structure refinement, it is thus evident that DCE can penetrate micropores, giving an indication that PDM isotherm models should be employed to fit the adsorption data. Moreover, this structural investigation can also explain the fact that the PDM model underestimates the adsorption capacity in comparison with that calculated from the solute density and adsorbent pore volume, especially as this finding has already been found in other studies [71]. Indeed, from the structural investigation, it appears that DCE cannot completely displace water from the micropores.

4. Conclusions

In this study, we investigated the adsorption process of 1,2-dichloroethane in an organophilic zeolite mordenite. A combined diffractometric, thermogravimetric, adsorption and gas chromatographic approach enabled clear evidence of DCE adsorption in the mordenite channel system to be obtained as well as to be localised the exact position occupied by the organic species in the structure. Rietveld refinement revealed the incorporation of 2.5 DCE molecules and approximately 4 water molecules per unit cell inside the mordenite channel system (about 10% in weight), in very good agreement with the weight loss given by TG analysis and with the saturation capacity which was determined from the adsorption isotherm. The water molecule oxygen atom distances from the organic molecule chlorine atoms (W–Cl1 = 2.34 Å, W–Cl2 = 2.53 Å) suggest that different DCE molecules could be connected by means of hydrogen bonds through W, to form a complex of DCE and water molecules independently by *gauche* or *trans* DCE sequencing.

The relevant incorporation of DCE molecules in the mordenite structure causes distortions of the 12-membered ring, where DCE are hosted, when compared to the parent zeolite. Structure refinement does not give clear indications as to whether only one or both *gauche*- and *trans*-conformers are present. Nevertheless, according to the results reported on 1-bromo-2-chloroethane in organophilic other zeolites [70] at room temperature, it is reasonable to assume a *trans* (*anti*) conformation for DCE in MOR.

Acknowledgment

The authors wish to thank Eni spa for their financial support. This work was also supported by PRRIITT (Emilia Romagna Region) misura 4 azione A.

References

[1] H. Muller, B. Deller, B. Despeyroux, E. Peldszud, P. Kammerhofer, W. Kuhn, R. Spielmannleitner, M. Stoger
Catal. Today, 17 (1993), pp. 383–390

[2] T.D. Hylton
Environ. Progr., 11 (1992), pp. 54–57

[3] R. Vignola, U. Cova, F. Fabiani, G. Grillo, R. Sbardellati, R. Sisto
Stud. Surf. Sci. Catal., 174 (Part 1) (2008), pp. 573–576

[4] R. Vignola, G. Grillo, R. Sisto, G. Capotorti, P. Cesti, M. Molinari, in: G.A. Boshoff, B.D. Bone (Eds.), Permeable Reactive Barriers, IAHS Publ 298, 2005, pp. 105–109.

[5] M.L. Occelli, H.E. Robson
Zeolite Synthesis
ACS Symposium Series American Chemical Society, Washington, DC (1989)

[6] R. Vignola, R. Bagatin, A. De Folly D'Auris, C. Flego, E. Previde Massara, M. Nalli, R. Sisto, in: C. Colella, P. Aprea, B. De Gennaro, B. Liguori (Eds.), IZC-IMMS 2010, A. De Fedre, Napoli, 2010, p. 51.

[7] S. Mizushima, Y. Morino, S. Noziri
Nature, 137 (1936), p. 945

[8] I. Nakagawa, S. Mizushima
J. Chem. Phys., 21 (1953), pp. 2195–2198

[9] S. Mizushima, T. Shimanouchi, I. Harada, Y. Abe, H. Takeuchi
Can. J. Phys., 53 (1975), pp. 2085–2094

[10] G. Georgieva, T. Dudev, B. Galabov, J.R. Durig
Vib. Spectrosc., 3 (1992), pp. 9–21

[11] R.J. Sabharwal, Y. Huang, Y. Song
J. Phys. Chem. B, 111 (2007), pp. 7267–7273

[12] J. Ainsworth, J. Karle
J. Chem. Phys., 20 (1952), pp. 425–427

[13] J.Y. Lee, N. Yoshida, F. Hirata
J. Phys. Chem. B, 110 (2006), pp. 16018–16025

[14] N.A. Murugan, H. Ågren
J. Phys. Chem. B Lett., 113 (2009), pp. 3257–3263

[15] R.J. Sabharwal, Y. Huang, Y. Song
J. Phys. Chem. B, 111 (2007), pp. 7267–7273

[16] M.W. Wong, M.J. Frisch, K.B. Wiberg
J. Am. Chem. Soc., 113 (1991), pp. 4776–4782

[17] B. Cohen, S. Weiss
J. Phys. Chem., 87 (1983), pp. 3606–3610

[18] E.G. Derouane
J. Mol. Catal. A Chem., 134 (1998), pp. 29–45

[19] M. Tajima, M. Niwa, Y. Fujii, Y. Koinuma, R. Aizawa, S. Kushiyama, S. Kobayashi, K. Mizuno, H. Ohuchi
Appl. Catal. B, 9 (1996), pp. 167–177

[20] J.R. González-Velasco, R. López-Fonseca, A. Aranzabal, J.I. Gutiérrez-Ortiz, P. Steltenpohl
Appl. Catal. B, 24 (2000), pp. 233–242

[21] E. Finocchio, C. Pistarino, S. Dellepiane, B. Serram, S. Braggio, M. Baldi, G. Busca
Catal. Today, 75 (2002), pp. 263–267

[22] R. López-Fonseca, S. Cibrián, J.I. Gutiérrez-Ortiz, J.R. González-Velasco
Stud. Surf. Sci. Catal., 142 (2002), pp. 847–854

[23] R. López-Fonseca, J.I. Gutiérrez-Ortiz, J.L. Ayastui, M.A. Gutiérrez-Ortiz, J.R. González-Velasco
Appl. Catal. B: Environ., 45 (2003), pp. 13–21

[24] C. Colella
Stud. Surf. Sci. Catal.
J. Čejka, H. van Bekkum, A. Corma, F. Schueth (Eds.), Introduction to Zeolite Science and Practice (third Rev.ed.), Elsevier, Amsterdam (2007), pp. 999–1035 No. 168

[25] M.A. Anderson
Environ. Sci. Technol., 34 (2000), pp. 725–727

[26] I. Braschi, S. Blasioli, L. Gigli, C.E. Gessa, A. Alberti, A. Martucci
J. Hazard. Mater., 178 (2010), pp. 218–225

[27] A. Martucci, L. Pasti, N. Marchetti, A. Cavazzini, F. Dondi, A. Alberti
Micropor. Mesopor. Mater., 148 (2012), pp. 174–183

[28] H. Van Koningsveld, F. Tuinstra, H. Van Bekkum, J.C. Jansen
Acta Crystallogr. B, 45 (1989), pp. 423–431

[29] D.H. Olson, G.T. Kokotailo, S.L. Lawton, W.M. Meier
J. Phys. Chem., 85 (1981), pp. 2238–2243

[30] G.D. Price, J.J. Pluth, J.V. Smith, J.M. Bennett, R.L. Patton
J. Am. Chem. Soc., 104 (1982), pp. 5971–5977

[31] H. Van Koningsveld
Acta Crystallogr. B, 43 (1987), pp. 127–132

[32] Y. Yokomori, S. Idaka
Micropor. Mesopor. Mater., 28 (1999), pp. 405–413

[33] H. Van Koningsveld, J.C. van Jansen
Micropor. Mesopor. Mater., 6 (1996), pp. 159–167

[34] G. Reck, F. Marlow, J. Kornatowski, W. Hill, J. Caro
J. Phys. Chem., 100 (1996), pp. 1698–1704

[35] B.F. Mentzen
J. Appl. Crystallogr., 22 (1989), pp. 100–104

[36] K. Nishi, A. Hidaka, Y. Yokomori
Acta Crystallogr., B61 (2005), pp. 160–163

[37] A. Rossner, S.A. Snyder, D.R.U. Knappe
Water Res., 43 (2009), pp. 3787–3796

[38] D.R.U. Knappe, A. Rossner, S.A. Snyder, C. Strickland, American Water Works Association
Research, Foundation, Denver, Colorado, 2007.

[39] A. Malka-Edery, K. Abdallah, Ph. Grenier, F. Meunier
Adsorption, 7 (2001), pp. 17–25

[40] O.H. Tezel, D.M. Ruthven, D.L. Wernick D. Olson, A. Bisio (Eds.),
Proc. 6th Intern Conf Zeolites, Butterworth, Guildford, UK (1984), pp. 232–241

[41] A. Germanus, J. Kärger, H. Pfeifer
Zeolites, 4 (1984), pp. 188–190

[42] C. Beauvais, A. Boutin, H. Fuchs
Adsorption, 11 (2005), pp. 279–282

[43] T. Tsuda, B.-W. Lu, H. Sasaki, Y. Oumi, K. Itabashi, T. Teranishi, T. Sano
Stud. Surf. Sci. Catal., 154 (2004), pp. 224–232

[44] L.B. Sand, Molecular Sieves, Conference Papers, 1967, Society of Chemical Industry, London, 1968, pp. 71–77.

[45] V. Sanders
Zeolites, 5 (1985), pp. 81–90

[46] F. Hamidi, A. Bengueddach, F. Di Renzo, F. Fajula
Catal. Lett., 87 (2003), pp. 149–152

[47] T. Armbruster, M.E. Gunter, in: D.L. Bish, D.W. Ming (Eds.),
Reviews in Mineralogy and Geochemistry Natural Zeolites: Occurrence Properties Use, vol. 45, Mineralogical Society of America, Washington, 2001, pp. 1–67.

[48] A. Alberti, P. Davoli, G. Vezzalini
Zeit. Kristallogr., 175 (1986), pp. 249–256

[49] P. Simoncic, T. Armbruster
Am. Miner., 89 (2004), pp. 421–431

[50] W.J. Mortier, J.J. Pluth, J.V. Smith
Mater. Res. Bull., 10 (1975), pp. 1319–1326

[51] A. Martucci, G. Cruciani, A. Alberti, C. Ritter, P. Ciambelli, M. Rapacciuolo
Micropor. Mesopor. Mater., 35–36 (2000), pp. 405–412

[52] A. Martucci, M. Sacerdoti, G. Cruciani, C. Dalconi
Eur. J. Miner., 15 (2003), pp. 485–493

[53] J.L. Schlenker, J.J. Pluth, J.V. Smith
Mater. Res. Bull., 14 (1979), pp. 751–758

[54] P. Simoncic, T. Armbruster
Micropor. Mesopor. Mater., 71 (2004), pp. 185–198

[55] H. Wang, Y. Huang
Langmuir (2009), pp. 8042–8050

[56] A. Boultif, D. Louër
J. Appl. Crystallogr., 24 (1991), pp. 987–993

[57] A.C. Larson, R.B. Von Dreele, General Structure Analysis System (GSAS), Los Alamos National Laboratory Report LAUR, 2000, pp. 86–748.

[58] B.H. Toby
J. Appl. Crystallogr., 34 (2001), pp. 210–213

[59] P. Thompson, D.E. Cox, J.B. Hastings
J. Appl. Crystallogr., 20 (1987), pp. 79–83

[60] M. Jaroniec, R. Madey,
Physical Adsorption on Heterogeneous Solid, Studies in Physical and Theoretical Chemistry, vol. 59, Elsevier, Amsterdam, The Netherlands, 1988, pp. 317–341.

[61] M. Manes
R.A. Meyers (Ed.), Encyclopedia of Environmental Analysis and Remediation, John Wiley, New York (1998), pp. 26–68

[62] R.M. Allen-King, P. Grathwohl, W.P. Ball
Adv.Water Res., 25 (2002), pp. 985–1016

[63] http://www.inchem.org/pages/sids.html.

[64] S. Kleineidam, C. Schüth, P. Grathwohl
Environ. Sci. Technol., 36 (2002), pp. 4689–4697

[65] S.W. Davis, S.E. Powers
J. Environ. Eng., 126 (2000), pp. 354–360

[66] G.R. Parker
Adsorption, 1 (1995), pp. 113–132

[67] A. Giaya, R.W. Thompson, R. Denkewicz
Micropor. Mesopor. Mater., 40 (2000), pp. 205–218

[68] Ch. Baerlocher, L.B. McCusker, D.H. Olson
Atlas of Zeolite Framework Types
(sixth Rev ed.)Elsevier, Amsterdam (2007)

[69] F. Porcher, E. Borissenko, M. Souhassou, M. Takata, K. Kato, J. Rodriguez-Carvajal, C. Lecomte
Acta Crystallogr., B64 (2008), pp. 713–724

[70] J.H. Leech, H. Wang, C. Granger, T. Woo, Y. Huang, in: Proceedings of the 19th Int Conference on Raman Spectroscopy, ICORS, 2004, Gold Coast, Queensland, Australia, 8–13 August 2004. (http://www.publish.csiro.au/issue/1051.htm).

[71] E. Bi, S.B. Haderlein, T.C. Schmidt
Water Res., 39 (2005), pp. 4164–4176